

BOSTON UNIVERSITY
COLLEGE OF ENGINEERING

Dissertation

A BU THESIS LATEX TEMPLATE

by

JOE CANDIDATE

B.S., Some University, 2016
M.S., Another University, 2018

Submitted in partial fulfillment of the
requirements for the degree of
Doctor of Philosophy

2024

© 2024 by
JOE CANDIDATE
All rights reserved

MS theses only: Prior to having this page signed by the readers, please have it reviewed by the Mugar Library staff. This does not apply to PhD dissertations since this page is completed through DocuSign. **Remove this comment in the final document** by commenting out `\approvalpagewithcomment` and uncommenting `\approvalpage` statements in the *prelim.tex* file.

Approved by

First Reader

First M. Last, PhD
Professor of Electrical and Computer Engineering

Second Reader

First M. Last
Associate Professor of ...

Third Reader

First M. Last
Assistant Professor of ...

*Facilis descensus Averni;
Noctes atque dies patet atri janua Ditis;
Sed revocare gradum, superasque evadere ad auras,
Hoc opus, hic labor est.* Virgil (from Don's thesis!)

Acknowledgments

Here go all your acknowledgments. You know, your advisor, funding agency, lab mates, etc., and of course your family.

As for me, I would like to thank Jonathan Polimeni for cleaning up old LaTeX style files and templates so that Engineering students would not have to suffer typesetting dissertations in MS Word. Also, I would like to thank IDS/ISS group (ECE) and CV/CNS lab graduates for their contributions and tweaks to this scheme over the years (after many frustrations when preparing their final document for BU library). In particular, I would like to thank Limor Martin who has helped with the transition to PDF-only dissertation format (no more printing hardcopies – hooray !!!)

The stylistic and aesthetic conventions implemented in this LaTeX thesis/dissertation format would not have been possible without the help from Brendan McDermot of Mugar library and Martha Wellman of CAS.

Finally, credit is due to Stephen Gildea for the MIT style file off which this current version is based, and Paolo Gaudiano for porting the MIT style to one compatible with BU requirements.

Janusz Konrad
Professor
ECE Department

A BU THESIS LATEX TEMPLATE

JOE CANDIDATE

Boston University, College of Engineering, 2024

Major Professors: First M. Last, PhD

Professor of Electrical and Computer Engineering
Secondary appointment

First M. Last, PhD
Professor of Computer Science

ABSTRACT

Have you ever wondered why this is called an *abstract*? Weird thing is that its legal to cite the abstract of a dissertation alone, apart from the rest of the manuscript.

Contents

1	Introduction	1
1.1	A few remarks before you start	1
2	The KamLAND-ZEN Experiment	3
2.1	KamLAND	3
2.1.1	Detector Infrastructure and Outer Detector	3
2.1.2	Inner Detector	5
2.1.3	Liquid Scintillator	8
2.1.4	KamLAND-ZEN and XeLS	8
2.2	Chemical Handling Infrastructure	9
2.2.1	Water Extraction	9
2.2.2	Distillation	9
2.2.3	Xenon Handling	10
2.3	Data Acquisition	10
2.3.1	KamLAND DAQ	10
2.3.2	KamFEE DAQ	11
2.3.3	MoGURA	12
2.4	KamLAND-ZEN Phases	13
2.4.1	KamLAND-ZEN 400	13
2.4.2	KamLAND-ZEN 800	14
2.4.3	KamLAND2-ZEN	17

3 KamLAND-ZEN Simulation and Reconstruction	21
3.1 Analysis Framework	21
3.1.1 Data Flow	21
3.2 Event Reconstruction	23
3.2.1 Waveform Analysis	23
3.2.2 PMT Corrections	24
3.2.3 Primary Vertex Fitter	27
3.2.4 Secondary Fitter	27
3.2.5 Energy Reconstruction	28
3.2.6 Bad Channels in Energy Reconstruction	30
3.2.7 Muon Reconstruction	32
3.2.8 Cosmic Ray Muon Reconstruction	33
3.2.9 MoGURA Neutron Reconstruction	34
3.2.10 Muon Neutron Correlation	35
3.3 Event Selection	36
3.3.1 Unphysical and Bad Quality Event Rejection	37
4 Conclusions	38
4.1 Summary of the thesis	38
A Proof of xyz	39
Curriculum Vitae	42

List of Tables

2.1	Composition and properties of KamLAND Liquid Scintillator (KamLS)	8
2.2	Composition of XeLS from three phases of KamLAND-ZEN	9
2.3	Film Contamination three phases of KamLAND-ZEN. Values taken from [8]	16

List of Figures

2.1	KamLAND site	4
2.2	KamLAND-ZEN detector	5
2.3	17-inch and 20-inch PMTs, both have the same footprint, but the 17-inch PMT photocathode is masked to a 17-inch diameter.	6
2.4	Quantum Efficiency of the KamLAND inner PMTs and PPO emission over wavelength. Figure taken from [7]	7
2.5	Flow diagram of the KLZ Xenon system. The purple lines denote the flow of Xe/XeLS, the blue line denotes the flow of decane, the grey line denotes the flow of LS. Figure from Reference	11
2.6	Flow diagram of the KamLAND data acquisition system, taken from [6]	12
2.7	Inner balloon structure and measurements for KamLAND-ZEN 800 configuration, taken from [8]	18
2.8	Coincidence event rate in KamLAND-ZEN 800 during the first distillation campaign, second distillation campaign, and Zenon loading phase. The red points denote ^{214}Bi and the blue points denote ^{212}Bi . Figure taken from [6].	19

2.9	Effective Majorana neutrino mass $m_{\beta\beta}$ as a function of the lightest neutrino mass $m_{lightest}$. The dark shaded regions are based on the best-fit neutrino oscillation parameters, while the lighter regions indicate 3σ ranges calculated from oscillation parameter uncertainties [3] [1]. The horizontal lines indicate various 90% C.L. upper limits on $m_{\beta\beta}$ from KamLAND-ZEN's ^{136}Xe results and a few different NME calculations. The blue bars on the right indicate three different theoretical predictions in the IO region. [2]	20
3.1	Data flow in KamLAND from raw waveforms to analysis variables such as energy, vertex, total hit PMTs, etc. [8]	22
3.2	An example of waveform analysis from thesis [10]. (left) ADC counts of a real waveform after baseline subtraction. The left cyan line is the leading edge, the center red line is the peak position, and the right dark cyan line is a trailing-edge. (right) Clock calibration example on 25 nsec intervals.	24
3.3	The trend in the number of low gain 17-inch PMTs, before ZEN-800. The number of low gain channels increased gradually, while the sudden increases are from HV reductions performed since 2017 [8].	25
3.4	An example pmt hit time distribution from data run 14783, the 50-100 ns leading window is taken to measure the pmt dark hit rate. [6].	26
3.5	Probability density function of 17-inch and 20-inch PMT hit times calculated from calibration data. The plot is from [8] and originally from a 2005 calibration dataset.	28
3.6	Fitting no hit probability to a low gain PMT against the expected charge μ . The original model is shown with the blue line while the red line is the new model which agrees better with low-gain PMT data.	32

3.7	A neutron capture events hit times showing the contribution of fake after pulses and the time windows used to calculate N_s	35
3.8	distribution showing the dT dependence of N_s . The events above the red line are selected as MoGURA neutrons and used for background rejection [9]	37
3.9	The dT distribution of selected MoGURA neutrons. The fit to an exponential is performed between 500 and 1000 μs . [9]	37

List of Abbreviations

As per BU library instructions, the list of abbreviations must be in alphabetical order by the **abbreviation**, not by the explanation, or it will be returned to you for re-ordering. **This comment must be removed in the final document.**

CAD	Computer-Aided Design
CO	Cytochrome Oxidase
DOG	Difference Of Gaussian (distributions)
FWHM	Full-Width at Half Maximum
LGN	Lateral Geniculate Nucleus
ODC	Ocular Dominance Column
PDF	Probability Distribution Function
\mathbb{R}^2	the Real plane

Chapter 1

Introduction

1.1 A few remarks before you start

Please read the short pointers below and on the subsequent pages; this will help you avoid frustrations when submitting the final dissertation to the library.

Your thesis should have 1.5in left and top margins, and 1in right and bottom margins. Getting this right is tricky since it may depend on your particular Latex installation. Most likely you will need to adjust some of the dimensions set up at the beginning of "bu_ece_thesis.sty" in this folder. Basically, every installation should have the base margin of 1in at the left and top, but this is not always the case. For example, the TexStudio/MiKTeX installation this document was set up on, has the default top margin of 0.3125in and so an additional margin of 0.6875in was added via \topmargin. In order to adjust these dimensions, you may want to follow these steps:

- compile the document into PDF,
- open the document in Acrobat Reader, set it to full-page viewing and magnification to 100%
- navigate to a "full" page with the text extending from the very top to the very bottom and full-width left to right,
- measure the margins and adjust accordingly,

- if you are planning to print a hardcopy, you need to make sure to select "Page scaling" to "None" in Acrobat.

Another issue that BU librarians may complain about and you are likely to encounter are long URLs or other unbreakable text. In case of long URL addresses, you should use the URL package; please see suitable documentation on-line.

However, if you encounter a long unbreakable word (e.g., foreign) the URL package does not help. Have a look at the example extending into the page margin:

Consider the following Java-JDT plugin name in German: "‘Plugin-Entwicklungsumgebung’".

Clearly, this is a problem, and BU librarians will complain. One way of fixing this issue is to enclose the offending paragraph in `\begin{sloppypar}` and `\end{sloppypar}`, resulting in the following outcome:

Consider the following Java-JDT plugin name in German: "‘Plugin-Entwicklungsumgebung’".

Indeed, although the paragraph spacing becomes sloppy, at least you can hand in the thesis!

LaTeX has a steep learning curve. You can use the original book by Lamport to learn more [5], but there are many on-line resources with excellent instructions and examples. Just Google a LaTeX topic you would like to explore.

As far as editing and compilation of LaTeX sources, if you have not found one yet, TexStudio seems to be quite popular.

Chapter 2

The KamLAND-ZEN Experiment

KamLAND, the **K**amioka **L**iquid-scintillator **A**nti **N**eutrino **D**etector, is a large liquid scintillator calorimeter detector situated 1km below mt. Ikenoyama in Gifu prefecture, Japan. I will describe the KamLAND detector's and the corresponding KamLAND experimental area's important components and features in this chapter. I will also explain how each component contributes to the KamLAND's scientific goals and the work of this thesis.

2.1 KamLAND

One can think of KamLAND as an onion made up of many spherical layers, each layer serving the ultimate goal of shielding and observing the central core, the xenon-loaded liquid scintillator.

2.1.1 Detector Infrastructure and Outer Detector

The KamLAND detector is surrounded by the KamLAND experimental area, situated in an old iron mine, multiple caverns and passageways were excavated and set aside for KamLAND experimental use.

The KamLAND site is shown in Figure 2.1. The control room contains networking and monitoring equipment which on-site shifters use to observe real-time detector activity. The first LS purification areas contain liquid-liquid extraction and nitrogen purge purification systems. The second LS purification area contains a distillation

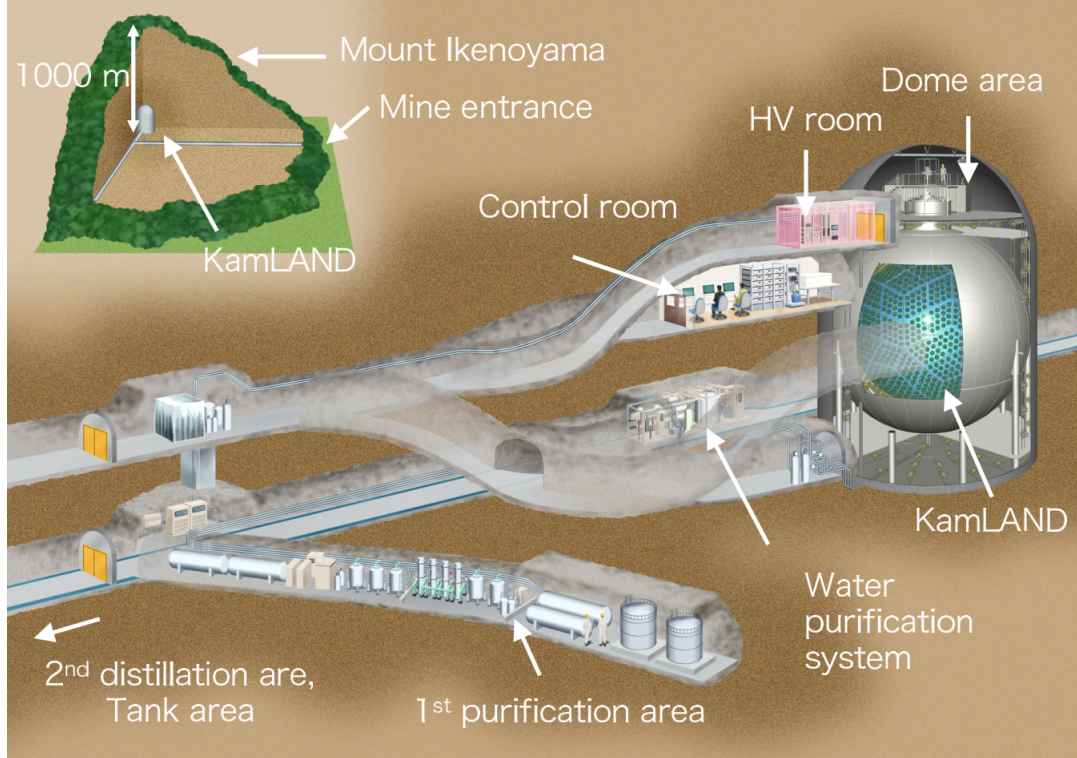


Figure 2.1: KamLAND site

purification system. A new Xenon purification area was built for KamLAND-Zen. The dome area is a class 1,000 clean area atop the detector and includes a calibration source preparation room and electronics enclosure (electronics hut or e-hut). At the center of the dome area, there is a secondary class 100-1000 clean tent covering the KamLAND chimney. The inner balloon installations took place in August 2016 and May 2018 inside this clean tent.

The outer detector (OD) is a cylindrical water tank 20m tall and with 20m diameter and filled with pure water. The OD was refurbished in 2016, and 140 new 20-inch PMTs (R3600) were installed inside the cavity. The inner wall of the outer tank and the outer surface of the inner detector stainless steel spherical tank are covered highly reflective Tyvek sheets (Tyvek 1073B and 1082D) to collect as much of the light generated by crossing cosmic ray muons as possible. The outer detector's role is

to tag cosmic ray muons, shield radioactivity and fast neutrons from the outer rock, and to stabilize the temperature of the ID.

2.1.2 Inner Detector

KamLAND's inner detector (ID) is the main spherical liquid scintillator detector, it is shown in Figure 2·2. The ID is contained in a 18m diameter stainless steel sphere tank. 1,879 PMTs are mounted onto the inner wall of the ID, 1,325 17-inch and 554 20-inch PMTs. The PMTs are submerged in non-scintillating buffer oil (BO). An acrylic panel separates the buffer layer into two shells. This panel prevents the convection of radon out-gassed from PMT glasses into the central parts of the detector.

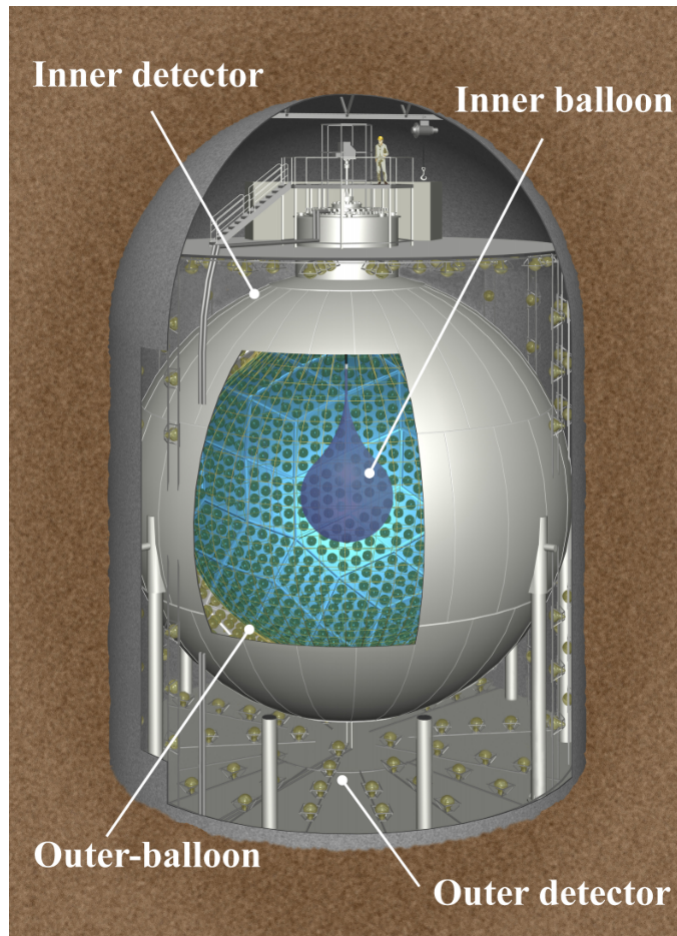


Figure 2·2: KamLAND-ZEN detector

Photomultiplier tubes (PMTs) are KamLAND’s eyes, detecting individual photons of light emitted by the passage of charged particles through the liquid scintillator volumes. Photons that hit PMT photocathodes are converted into a photoelectron. This photoelectron is then guided by electric fields to a series of dynodes. Each dynode multiplies the photoelectrons many times over, until the first photoelectron becomes 10^{6-7} electrons. Should multiple photons hit the photocathode simultaneously, the output voltage increases proportionally. This current is converted to a voltage by a coupling capacitor and read out via long coaxial cables. Figure 2·3 is a diagram of the 17in and 20in PMTs.

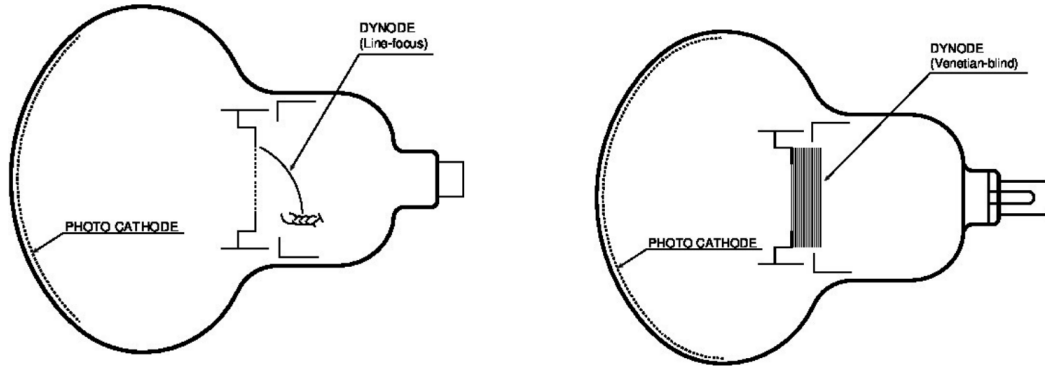


Figure 2·3: 17-inch and 20-inch PMTs, both have the same footprint, but the 17-inch PMT photocathode is masked to a 17-inch diameter.

The 1,325 17-inch PMTs are Hamamatsu R7250s while the 554 20-inch PMTs are Hamamatsu R1449s and R3600s. The 20-inch PMTs were inherited from the Kamiokande experiment to increase our light collection. Both sets of PMTs have a bialkali photocathode sensitive to 300-650nm light which is well-suited for the emission spectrum of the LS. The pmts also differ by dynode design; while the 17-inch PMTs feature "box-and-line" designs, the 20-inch PMTs have "venetian-blind styles". The different dynode designs along with the masking on the 17-inch PMTs, give us 17-in PMTs with better transit time spread (TTS) and 20-inch PMTs with better light collection efficiency. In total, the photocathode coverage of the ID is 34%, with 23%

contributed by the 17-inch PMTs.

Furthermore, the PMT performance can be affected by the earth's magnetic field. To reduce this unwanted effect, the entire KamLAND detector is surrounded by geomagnetic compensation coils to counteract this external magnetic field. The residual magnetic field is less than 50mG, which has negligible effect on the PMT performance.

Another important characteristic of PMTs is their quantum efficiency (QE). The QE quantifies the probability that a photon arriving on the photocathode will produce a photoelectron. A PMT's QE varies over the wavelength of the incoming light. To improve our light collection, KamLAND's LS is doped with PPO to shift the wavelength of the incoming light to where the PMTs are most sensitive. Figure 2.4 shows the PMT QE curve and the PPO reemission spectrum.

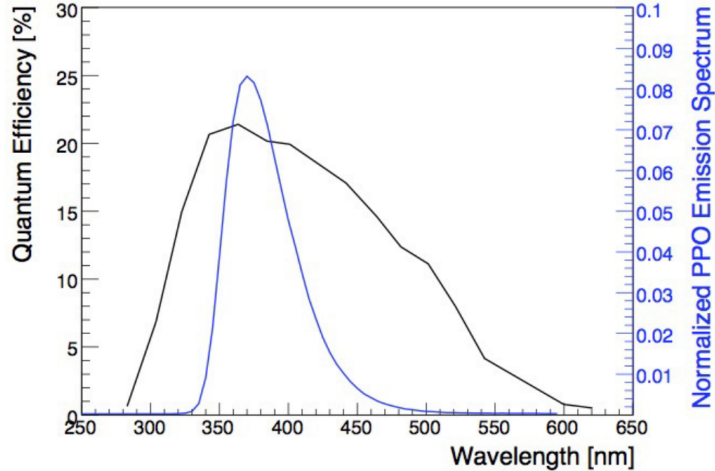


Figure 2.4: Quantum Efficiency of the KamLAND inner PMTs and PPO emission over wavelength. Figure taken from [7]

Next, is the 13m diameter outer balloon (OB). The OB is suspended in the center of the ID within the buffer oil, it is filled with one kiloton of highly purified organic liquid scintillator.

2.1.3 Liquid Scintillator

Liquid scintillator (LS) is the vital medium that sensitizes KamLAND to internal radioactivity. The KamLAND LS (KamLS), found in between the outer balloon and inner balloon, is composed of 80.2% of dodecane (D12), 1,2,4-trimethyl benzene, and 19.8% pseudocumene (PC). A wavelength shifter called 2,5-diphenyloxazole (PPO) is added to the LS at a concentration of 1.36 ± 0.03 g/L. KamLAND-Zen has achieved 5×10^{-18} g/g and 1.3×10^{-17} g/g contamination for ^{238}U and ^{232}Th , respectively.

The chemical composition of the KamLS can be found in Table 2.1

	D12	PC	PPO
Chemical Formula	C ₁₂ H ₂₆	C ₉ H ₁₂	C ₁₅ H ₁₁ NO
Density [g/cm ³]	0.7526	0.8796	-
Boiling Point [°C]	216	169	360
Melting Point [°C]	-10	-44	72
Flash Point [°C]	83	54	-

Table 2.1: Composition and properties of KamLAND Liquid Scintillator (KamLS)

2.1.4 KamLAND-ZEN and XeLS

At the center of KamLAND-ZEN lies the Xenon-loaded Liquid Scintillator (XeLS) contained in the 1.9m radius inner balloon (IB). The double-beta decaying isotope ^{136}Xe is thus placed in the cleanest, most sensitive part of the experiment. The Xenon gas is enriched to 90% ^{136}Xe and is dissolved into a modified version of KamLS. The PPO concentration was increased to 4g/L to boost the light yield. This increased PPO concentration compensates for the 10% reduction in emitted scintillation light when Xenon is mixed into the LS. The XeLS density is also tuned to match the surrounding KamLS. The chemical composition of the XeLS is shown in Table 2.2 in each of the different phases of the KamLAND-ZEN experiment.

Material	Decane (%)	PC (%)	PPO (%)	Xe (%)
Zen 400 Phase-1	82.3	17.7	2.7	2.44/2.48
Zen 400 Phase-2	80.7	19.3	2.29±0.03	2.91
Zen 800	82.4	17.6	2.38±0.02	3.13

Table 2.2: Composition of XeLS from three phases of KamLAND-ZEN

2.2 Chemical Handling Infrastructure

Background mitigation is crucial for $0\nu\beta\beta$. Maintaining the purity of the liquid volumes inside KamLAND is an important part of background mitigation in KamLAND-ZEN. In this section, we will briefly describe the systems that provided or maintain the purity of the LS and XeLS in KamLAND.

2.2.1 Water Extraction

The first purification is shown in Figure ???. Both the liquid scintillator and buffer oil are filtered in two stages with $1\mu\text{m}$ and $0.1\mu\text{m}$ pore sizes respectively. Next, the liquids are flushed with pure water in the water extraction tower where metals such as U, Th, and K, are absorbed by the water. Finally, the liquids are purged with ultra-pure nitrogen gas to remove gaseous contaminants like radon and oxygen.

2.2.2 Distillation

The next purification system utilizes the distillation system shown in Figure ???. LS from KamLAND is constantly cycled through the distillation system. There boiling is done to separate the individual chemical components of KamLS, namely Pseudocumene (PC) and PPO. Each component is individually distilled and purified. Then, the components are combined in the mixing tank to the original LS composition with an accuracy of 10^{-3}g/cm^3 . Finally high-purity nitrogen gas is used to purge the LS coming out of the mixing tank to eliminate any gaseous contaminants.

2.2.3 Xenon Handling

A schematic diagram of the XeLS handling system is shown in Figure 2.5. The system consists of the following components:

- A **1.1 m³ Main Tank** directly connected to KamLAND-ZEN’s inner balloon. The extracted XeLS first enters this tank.
- A **1.1 m³ Reservoir Tank** that is connected to the main tank via a vacuum pump and LS trap. It is refrigerated with liquid N₂ to -50°C, at which the LS gas is condensed and trapped. Only Xe gas is allowed to flow into the reservoir tank.
- A **25 m³ Storage Tank** is connected to the main tank. The degassed LS is poured into this tank for storage.
- A **1.1 m³ Sub-tank** is also connected to the main tank, the detector, the control tank, and the purified Xe gas system. The Xe gas is mixed into LS inside this tank. The density of chemical cocktails in the sub-tank is monitored and adjusted by the control tank. After mixing, the XeLS is filtered and fed back into the balloon.
- A **1.1 m³ Control Tank** is directly connected to the second purification area. The control tank controls the density in the sub-tank by adjusting the Decane percentage. The control tank is pressurized with Nitrogen gas.

2.3 Data Acquisition

2.3.1 KamLAND DAQ

KamLAND uses two data acquisition (DAQ) systems in parallel. The first is KamFEE (KamLAND Front End Electronics), which has been used since the start of

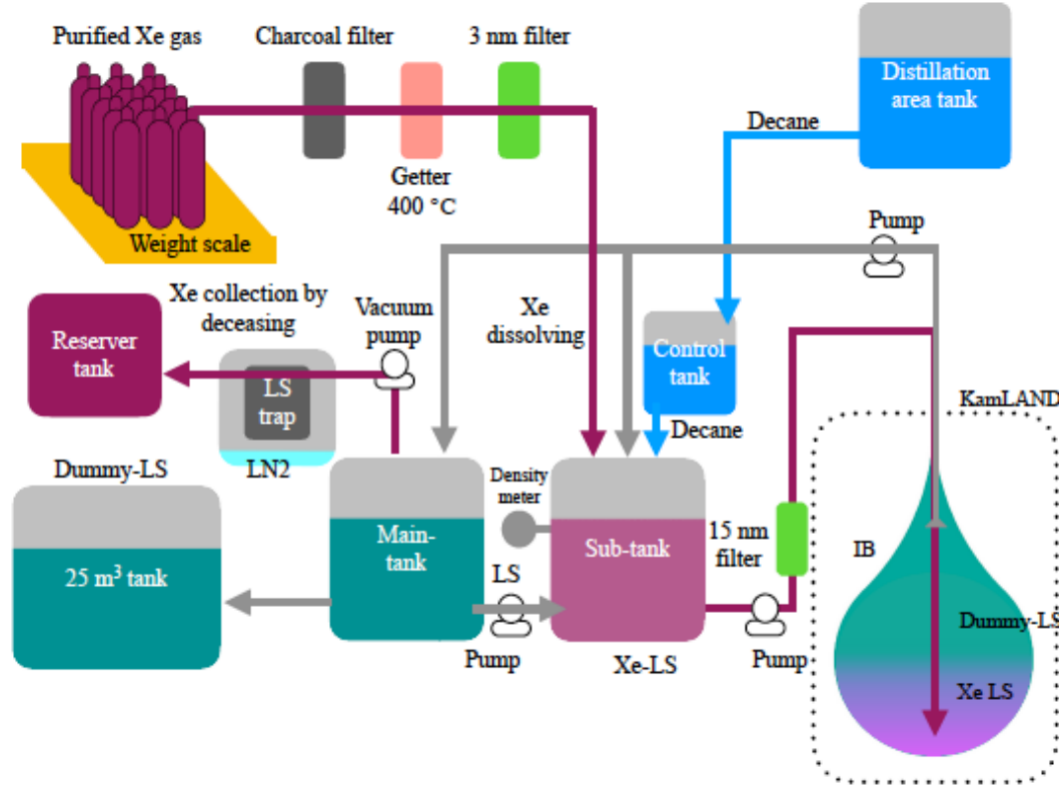


Figure 2.5: Flow diagram of the KLZ Xenon system. The purple lines denote the flow of Xe/XeLS, the blue line denotes the flow of decane, the grey line denotes the flow of LS. Figure from Reference

KamLAND physics data-taking. The other is MoGURA (Module for General-Use Rapid Application). MoGURA is a data acquisition system developed to eliminate the deadtime just after cosmic ray muon events. An overview of this dual scheme data acquisition system is shown in 2.6. What follows is a brief description of each DAQ system.

2.3.2 KamFEE DAQ

KamFEE are the front end electronics that read and control the KamLAND PMTs. The boards are of VME 9U form factor and are synchronized with a 40 MHz clock. The PMT signals are sent along two parallel channels. The first channel is sent to a

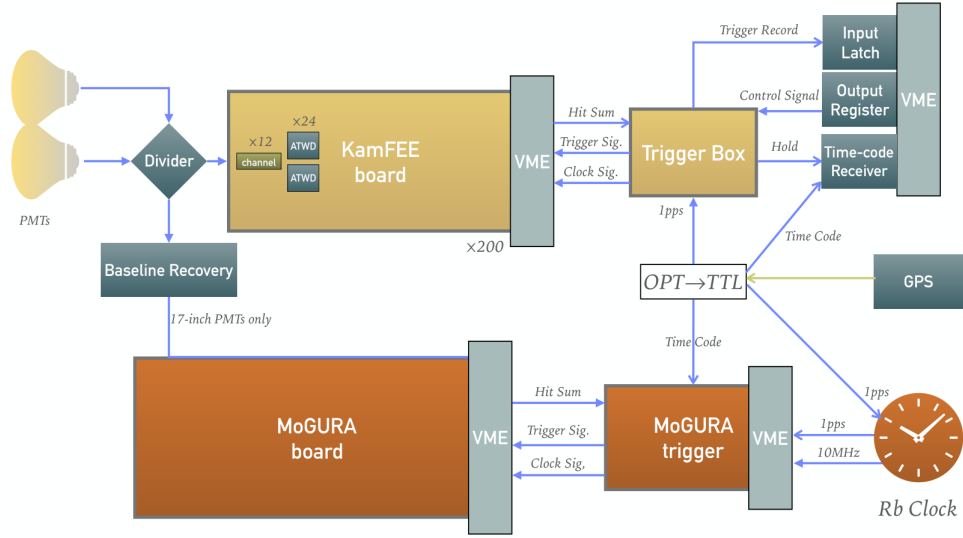


Figure 2·6: Flow diagram of the KamLAND data acquisition system, taken from [6]

discriminator which register a PMT hit if the voltage exceeds a predetermined value that corresponds to approximately 1/6th of a single photoelectron. The second channel, is delayed to give some time to process the discriminator signal and is fed into 3 amplifier stages (x20, x4, x0.5), this amplified signal is digitized by two analog Transient Waveform Digitizers (ATWDs). The ATWD is a 10-bit digitizer and samples every 1.5ns, 128 times per waveform. Each pulse takes 128 μ sec to digitize.

The KamFEE boards send a "hitsum" signal to the central KamFEE DAQ trigger, communicating a certain number of hits were received and can be digitized. The trigger board sends a signal back which issues the digitization command to the ATWDs. While the ATWD is digitizing, it cannot record further signals, therefore, two ATWDs are assigned to each channel to reduce deadtime.

2.3.3 MoGURA

MoGURA is the secondary data acquisition system in KamLAND; it is responsible for after pulses and dealing with PMT waveform overshoots caused cosmic muons.

KamLAND has a cosmic muon rate of 0.3 Hz, so it is important to compensate for the effects these high-energy events have on our detector. To accomplish this task, MoGDAQ has a few extra features over KamFEE.

- **Baseline Recovery:** After a high energy muon passes through the detector, the DAQ channels are saturated, which means the voltage exceeds the digitization window, so only the maximum value is read. Simultaneously, the voltage “overshoots” as it returns to normal and swings below the nominal value causing difficulties in digitizing signals that occur soon after these muons.
- **Adaptive mode:** Activates a special trigger mode after muon events to compensate for large after-pulses post-muon. This special trigger is based on differential PMT hits.

MoGURA data is used to tag neutrons created from muon spallation. These tagged spallation neutrons are vital in subsequent analyses to tag events that likely originated from these cosmic ray muons. The baseline restoration and neutron tagging will be further improved with the implementation of MoGURA2 trigger system. This is a planned replacement of the KamLAND data acquisition system (KamFEE and MoGDAQ both) for the KamLAND2-ZEN experiment, which is planned to begin physics data-taking in 2028.

2.4 KamLAND-ZEN Phases

The KamLAND-ZEN experiment has undergone multiple phases and renovations.

2.4.1 KamLAND-ZEN 400

The inner balloon and XeLS was added to the KamLAND experiment in 2011, starting the phase referred to as KamLAND-ZEN 400. This phase of the detector featured

a 3m diameter inner-balloon filled with liquid scintillator loaded with 3% Xenon by weight. The dissolved Xenon gas had 91% proportion of Xe¹³⁶.

The KamLAND-ZEN 400 data was split into two data-taking periods. Period-I data was contaminated with a high background of Ag^{110m}, the silver appeared to be leeching from the mini-balloon into the XeLS. The Ag^{110m} contamination on the inner balloon was likely due to nuclear fallout from the Fukushima reactor meltdown. The Fukushima meltdown occurred when the inner balloon was being manufactured and in the same geographical region of Japan. Period II started after the XeLS distillation suppressed the Ag^{110m} by a facator of 20. Period II continued data taking for 534.5 total livedays and the combined physics result of Periods I and II produced a $0\nu\beta\beta$ half-life limit of $T_{1/2}^{0\nu} > 1.07 \times 10^{25}$ years at 90% C.L. This half-life limit corresponds to an effective majorana mass limit of $m_{\beta\beta} < 61 - 165$ meV.

2.4.2 KamLAND-ZEN 800

KamLAND-ZEN 800 was the second phase of KamLAND-ZEN. KamLAND-ZEN took data from January 2019 to August 2024. Over 2kton·yrs of exposure was observed. KamLAND-ZEN 800 was decommission in Fall 2024, and is currently being disassembled.

Inner Balloon Manufacturing

KamLAND-ZEN 800 featured a larger, cleaner inner balloon which was fabricated at Tohoku University in a Class 1 cleanroom. The inner balloon is made from panels of 25 μm nylon-6. Innerballoon fabrication consisted of multiple steps some of these critical steps are listed here:

- **Washing** - the film is cleaned twice in an ultrasonic bathtub, then stored between cover films to prevent dust adhesion

- **Welding** - the cleaned balloon panels are welded with a semi-automatic welding machine. For delicate areas, such as the balloon neck, a hand welding machine was used. The average tensile strength on the balloon surface was 35 N/cm after welding.
- **He Leak Check** - Inevitably leaks will occur during the previous assembly procedures. Helium gas was pumped into the balloon to check for these leaks. The cover film of the balloon was peeled off before this leak check. Found leaks were repaired by patching the film. Over 900 leaks were found during the leak check.
- **Folding** - The inner balloon was folded into a cylinder shape and covered with sheath films to prevent contamination during transport. Teflon sheets and Vectran strings were used to tie the rolled balloon up for shipping.
- **Shipping** - The inner balloon was shipped within a silver gas bag. All corresponding tools were also shipped in airtight bags.

The inner balloon was installed on May 10, 2018. A rehearsal installation was performed in a swimming pool before the final deployment. In the final installation, the balloon is deployed through the 50cm port on the neck of the KamLAND detector. After filling the balloon with KamLS, the Teflon sheets, sheath films, and Vectran strings are pulled out of the detector. The whole operation was monitored in real-time via cameras and endoscope.

The top of the inner balloon is connected to a corrugated tube made from PEEK (poly-ether-ether-ketone). Twelve suspending belts support the inner balloon, wrapping around the full height of the balloon. The tension of each of these belts are monitored in real time to guarantee the position and stability of the balloon. A schematic of the balloon structure can be seen in Figure 2.7.

Contamination Control

Once deployed and exposed to the KamLAND scintillators, the inner balloon is very difficult to clean. Thus, maintaining balloon cleanliness is vital. After deployment, the IB was filled with distilled LS while the ^{232}Th level was measured at 10^{-15} g/g , exceeding the target background concentration. The PPO distillation tower was suspected to be a source of contamination and was investigated. ICP-MS and neutron activation analysis were used to measure ^{232}Th contamination at different locations along the distillation system. After meticulous washing and filter replacement, LS purification began to lower the ^{232}Th background. After two separate distillation campaigns, ^{238}U and ^{232}Th levels were reduced by a factor of 10 compared to KamLAND-ZEN 400. The contaminations can be estimated by performing a $^{214}\text{Bi}-^{214}\text{Po}$ and $^{212}\text{Bi}-^{212}\text{Po}$ coincidence analysis. The coincidence event rates plotted over time are shown in Figure 2.8 and listed in Table 2.3.

	^{238}U (10^{-17} g/g)	^{232}Th (10^{-17} g/g)
Zen 400 Phase-1	13 ± 2	190 ± 20
Zen 400 Phase-2	17 ± 1	5.5 ± 0.3
Zen 800	1.5 ± 0.4	30 ± 4

Table 2.3: Film Contamination three phases of KamLAND-ZEN. Values taken from [8]

KamLAND-ZEN 800 was decommissioned in 2024 after observing over 2 kiloton·yrs of exposure. The final half-life limit was reported as $T_{1/2}^{0\nu} > 3.8 \times 10^{26}$ years at 90% C.L. This half-life limit corresponds to an effective majorana mass limit range of 28–122 meV. As of Summer 2025, this is the world-leading limit on effective majorana mass from any double-beta decay isotope and is the only limit in the Inverted Mass Ordering region. The latest limits from KamLAND-ZEN800 are shown in Figure 2.9

2.4.3 KamLAND2-ZEN

KamLAND2 is the next generation of the KamLAND experiment, it will be built in the same detector cavern as KamLAND1. KamLAND2-ZEN will reach a goal limit of $T_{1/2}^{0\nu\beta\beta} > 2 \times 10^{27}$ yrs.

Most of the detector components will be replaced going from KamLAND to KamLAND2. Some of the more notable upgrades are:

- **Inner Detector PMTs** - All of the 1,879 inner PMTs will be replaced with modern low-TTS, high quantum efficiency (QE) phototubes.
- **Light Collecting Mirrors** - Light collecting winston cones will be attached to each of the PMTs to achieve virtually 100% photocoverage. These improvements will contribute to a goal energy resolution of 2%. This energy resolution will lead to a x100 reduction in the $2\nu\beta\beta$ background rate.
- **Improved Inner Balloon** - The new innerballon will be made up of PEN (polyethylenenaphthalate) which will scintillate from film radioactive backgrounds
- **MoGURA2** - Replace the 2 DAQ systems with MoGURA2, a newly developed, compact, dead-time free, RFSoC electronics.

KamLAND2-ZEN is scheduled to begin data-taking in 2028.

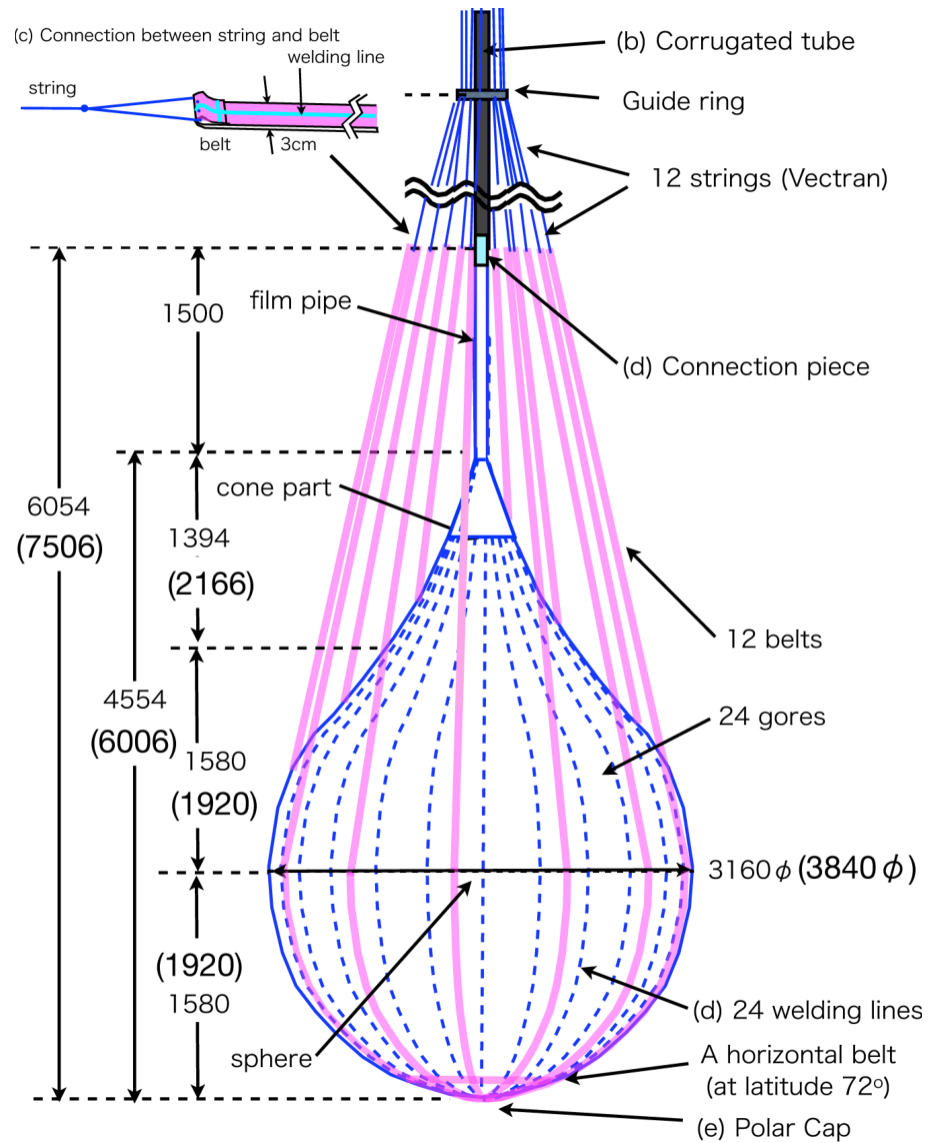


Figure 2·7: Inner balloon structure and measurements for KamLAND-ZEN 800 configuration, taken from [8]

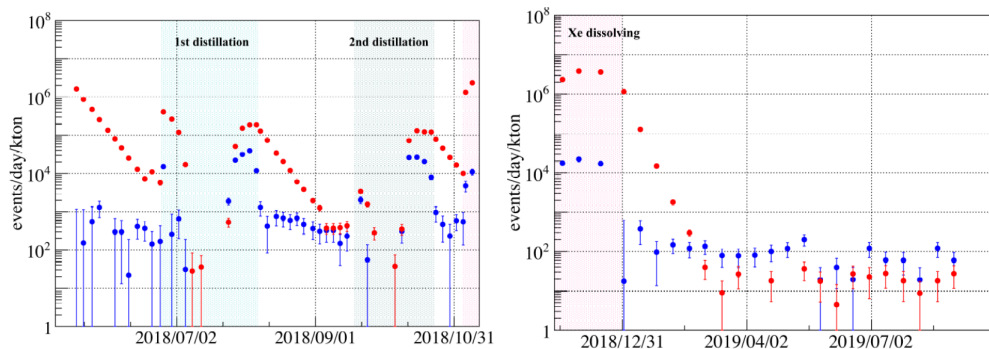


Figure 2·8: Coincidence event rate in KamLAND-ZEN 800 during the first distillation campaign, second distillation campaign, and Zenon loading phase. The red points denote ^{214}Bi and the blue points denote ^{212}Bi . Figure taken from [6].

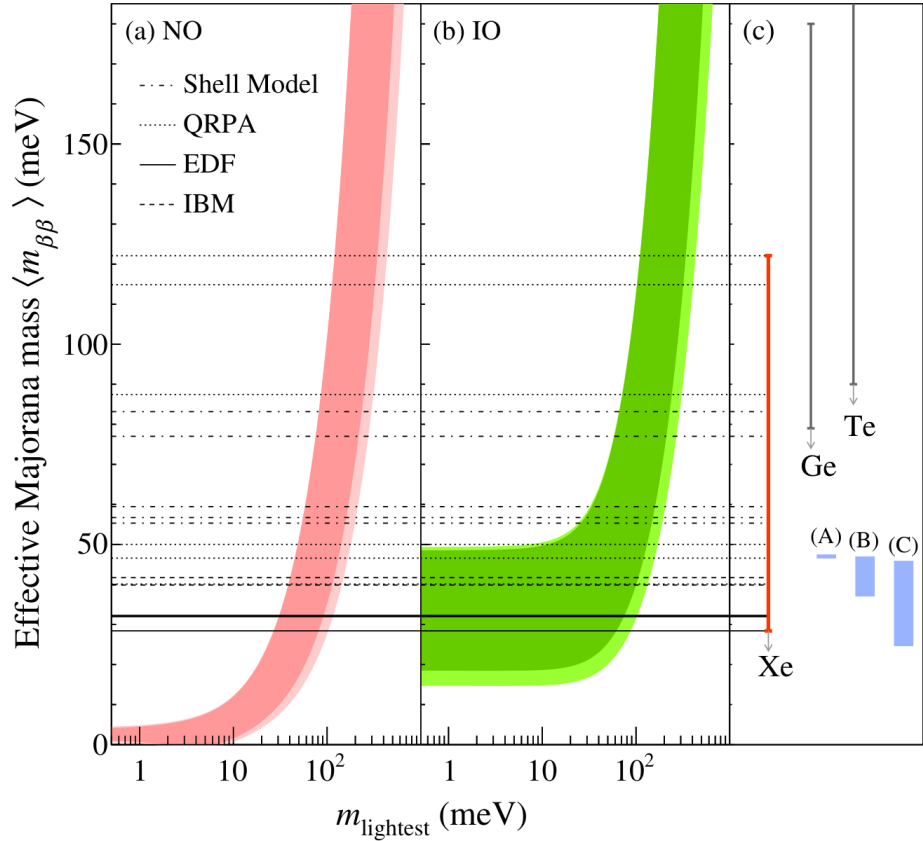


Figure 2.9: Effective Majorana neutrino mass $m_{\beta\beta}$ as a function of the lightest neutrino mass m_{lightest} . The dark shaded regions are based on the best-fit neutrino oscillation parameters, while the lighter regions indicate 3σ ranges calculated from oscillation parameter uncertainties [3] [1]. The horizontal lines indicate various 90% C.L. upper limits on $m_{\beta\beta}$ from KamLAND-ZEN's ^{136}Xe results and a few different NME calculations. The blue bars on the right indicate three different theoretical predictions in the IO region. [2]

Chapter 3

KamLAND-ZEN Simulation and Reconstruction

KamLAND-ZEN uses detailed simulations defined in KLG4Sim, a GEANT4-based Monte Carlo (MC) simulation software. The MC simulated events are tuned with real calibration events to carefully match real detector response. Simulated and physical events produce detector responses that are reconstructed to extract higher-level information such as energy and position. The reconstructed event information is used for data-selection and spectrum fitting. This chapter discusses the MC simulation and event reconstruction procedures used in KamLAND-ZEN 800.

3.1 Analysis Framework

3.1.1 Data Flow

Figure 3·1 outlines the data flow in KamLAND-ZEN. PMT signals are digitized in either KamFEE or MoGURA, the two DAQ systems discussed in the previous chapter, the digitized signals are stored in Kinoko Data Format (KDF). KDF files contain trigger information and timestamped, digitized PMT waveforms. KDF files also store run condition information in the header. The EventBuilder collates the waveforms of a single event and stores them in a serial file. A waveform analyzer reconstructs a hit time and charge (TQ) information for each of these waveforms. The RTQ files hold the Raw-TQ information for each PMT. Event vertices and visible energy are derived from the RTQ files through their respective reconstruction algorithms. There are

secondary reconstructions that are also applied to the RTQ files, such as muon track fitting, flasher vetos, double pulse fit, and unphysical event selections. The general vector file (GVF) is used for the main physics analyses like the one presented in this thesis.

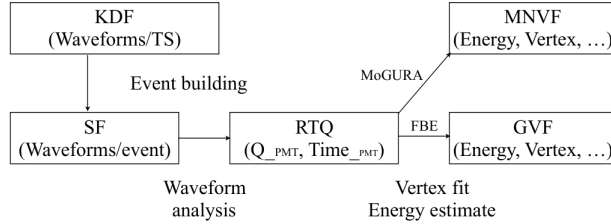


Figure 3.1: Data flow in KamLAND from raw waveforms to analysis variables such as energy, vertex, total hit PMTs, etc. [8]

GVF files contain the following information:

- **run number**
- **event number**
- **TimeStamp** based on DAQ clock time (25 nsec for KamFEE, 20 nsec for MoGDAQ)
- **unixtime** is the number of seconds from January 1st in 1970 and used for some run vetos
- **trigger type** records which trigger was used
- **event vertex and badness** event vertices and a radius from detector center is saved, along with a vertex fit quality parameter called badness
- **energy/energy17** visible energies given by the fitter, energy17 is the energy estimate only using 17-inch PMTs
- **TotalChargeID/17/OD** sum of all PMT charges of each PMT type

- **numhit/numhit17** the number of hit PMTs/17-inch PMTs in each event.
- **NsumMax** a maximum number of hit PMTs in a single DAQ cycle within each event, a "peak" nhit of the event
- **N200OD** Maximum number of simultaneous hit OD pmts within 200nsec windows
- **muon entrance and direction** muon fitter results are recorded.

Finally, MoGURA events are associated with muon events acquired in KamFEE DAQ (FBE) and stored in a Muon-Neutron Vector File (MNVF) to search for neutron capture events that occur shortly after muons.

3.2 Event Reconstruction

3.2.1 Waveform Analysis

Each digitized waveform has 128 samples with 1.5ns sample times; this corresponds to a waveform digitization window of 192 ns. The waveforms are processed and TQ reconstructed with the following procedure.

- **Smoothing** Each waveform is smoothed via a running-average first derivate.
- **Baseline adjustment** The baseline of each PMT is collected at the beginning of each run. This baseline is subtracted from each waveform.
- **Peak finding** Peaks are found with running-averaged 1st, 2nd, and 3rd derivatives.
- **Leading-edge and Trailing-edge tag** A leading-edge is stamped as 10ns before the peak voltage. The trailing edge is stamped when the waveform returns to baseline. An example of this time-stamping is shown in Figure 3.2

- **Waveform Sum calculation** The waveform is integrated from the leading-edge to the trailing-edge.

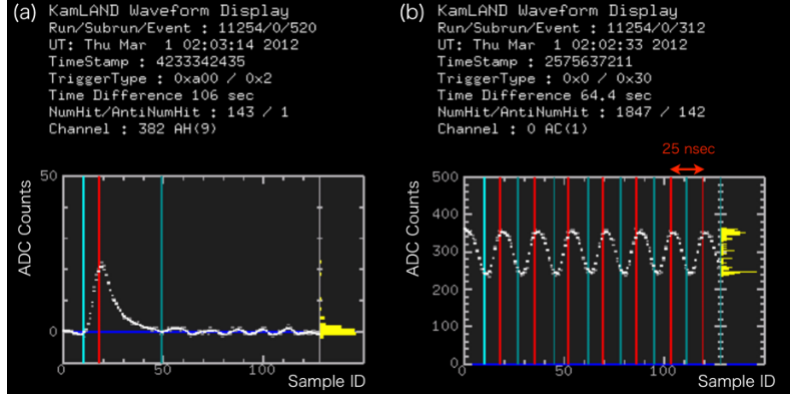


Figure 3.2: An example of waveform analysis from thesis [10]. (left) ADC counts of a real waveform after baseline subtraction. The left cyan line is the leading edge, the center red line is the peak position, and the right dark cyan line is a trailing-edge. (right) Clock calibration example on 25 nsec intervals.

When there are mulitple hits in one PMT waveform, the total charge of the hits and the earliest hit time is returned. This simplified information is used for the vertex and energy reconstruction. The multi-pe information is used for a double-pulse fit and a muon shower tag.

3.2.2 PMT Corrections

Low Gain Problem and HV Reductions

Since 2011, we observed that the gain of some of the 17-inch PMTs gradually decreased. As the gain of the PMTs fell, this compormises signal/background ratio and PMT waveform quality. It was also observed that the PMTs enter a low impedance state before the gain dropped. A HV current and voltage monitor allows for the real-time monitoring of this state. Usually a simple HV power cycle could recover normal PMT behavior. Since 2016, a auto HV power cycle mechanism was implemented to mitigate the low gain problem, but the root case is still unknown.

Each time the PMTs enter the low impedance state, the HV on that channel was reduced in 50-100 V increments. Over time, some of the channels had their HV reduced by 450 V. Figure 3.3 shows the trend in low gain 17-inch PMTs.

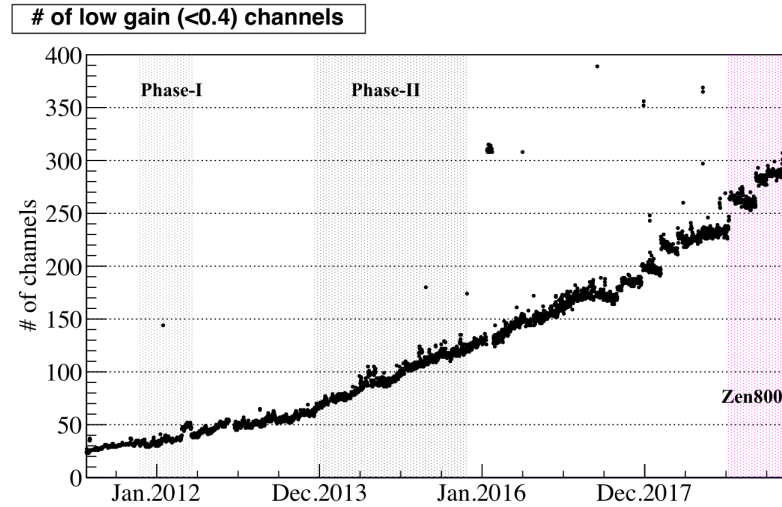


Figure 3.3: The trend in the number of low gain 17-inch PMTs, before ZEN-800. The number of low gain channels increased gradually, while the sudden increases are from HV reductions performed since 2017 [8].

Note about current low pmt gain analysis.

Bad Channel

A channels is considered bad if the PMT meets one or more of the following criteria:

- PMT pulses less than 0.6% of the time over all events
- PMT pulses below 0.48% for non-muon events
- PMT pulses less than 80% of the time for high-energy muon events
- PMT is missing a waveform more than 10% of the time
- Large discrepancy between the two ATWD hits

- High muon charge PMTs. A PMT may read much higher charge ($Q_{detected}$) than the average of its surrounding PMTs ($Q_{expected}$). A run is divided into 100 muon intervals, for each interval the criteria is defined as

$$\frac{1}{N_{interval}} \sum_{i=1}^{N_{interval}} \left(\frac{1}{N_{muon}} \sum_{j=1}^{N_{muon}} \frac{(Q_{expected} - Q_{detected})^2}{Q_{expected}} \right) > 1000 \text{ p.e.}$$

These bad channels are excluded from event reconstruction and physics analyses.

Dark Hit

Thermal fluctuations can emit electrons off the photocathode leading to a PMT hit signal. These "dark hits" are an unavoidable hit-level background in PMT detectors, lowering the detector temperature reduces this effect. The dark hit rates are measured from run-to-run and are factored into our likelihood-maximizing reconstruction algorithms. The hit rate observed 50-100 ns before the PMT hittime rising edge is taken as the dark rate, Figure 3·4 shows the PMT hittime distribution and the dark rate window.

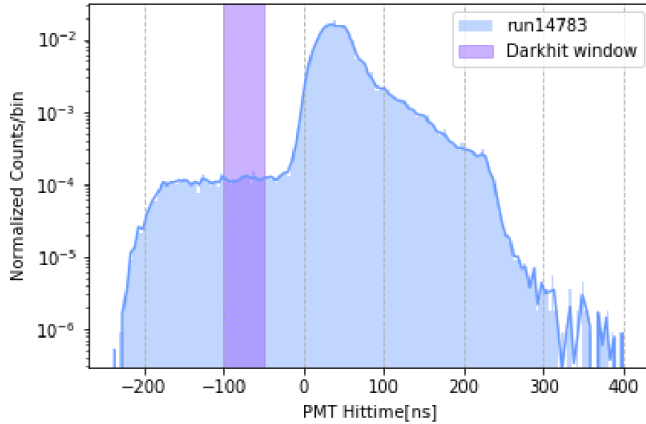


Figure 3·4: An example pmt hit time distribution from data run 14783, the 50-100 ns leading window is taken to measure the pmt dark hit rate. [6].

3.2.3 Primary Vertex Fitter

The primary vertex fitter provides a rough estimate of a scintillating event's location. This estimate serves as the input to a more thorough, but complex secondary fitter. The fit works by constructing a hit time residual distribution:

$$T_i^{emit} = T_i - TOF_i = T_i - \frac{|R_i - r_{vertex}|}{c_{eff}} \quad (3.1)$$

Here T_i is the hit time of the i^{th} PMT, TOF_i is the time it takes for a scintillation photon to traverse from the vertex position to the i^{th} PMT position, R_i is the PMT position, r_{vertex} is the unknown vertex position to fit for, and c_{eff} is the speed of light in the given medium. By fitting T_i^{emit} to match the standard scintillation time profile, a primary r_{vertex} is produced by the fitter.

3.2.4 Secondary Fitter

The secondary V2 fitter uses the r_{vertex} given by the primary fitter to compute T_0 according to the equation 3.2

$$T_0 = \frac{\sum_i (T_i^{pmt} - TOF_i^{pmt}) \times Q_i}{\sum_i Q_i} - const. \quad (3.2)$$

This T_0 is the charge weighted sum of T_{emit} from 3.1. This T_0 serves as the universal start point of an event. From this time, each pmt hit time is

$$\tau(x, y, z, T_0) = T_i^{pmt} - TOF_i^{pmt} - T_0 \quad (3.3)$$

Finally, these time-of-flight corrected and centered hit time distributions are used to create probability distributions for the 17 and 20 inch PMTs respectively. These PDFs are shown in Figure 3.5. The likelihood function for an individual PMT is

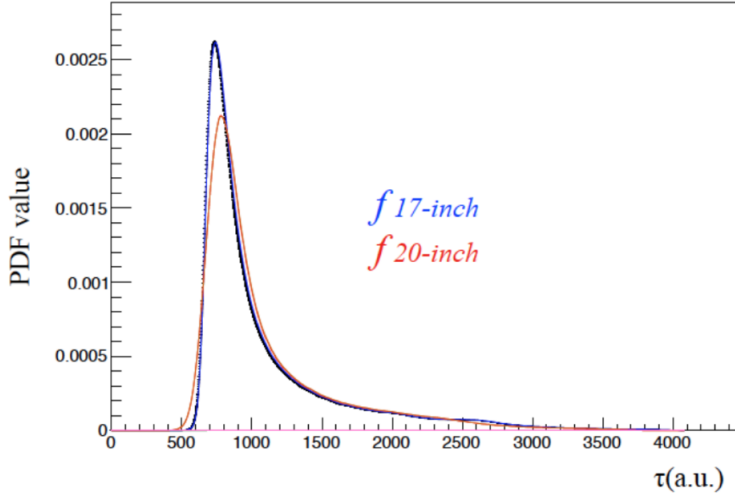


Figure 3.5: Probability density function of 17-inch and 20-inch PMT hit times calculated from calibration data. The plot is from [8] and originally from a 2005 calibration dataset.

defined as:

$$\phi_i = \frac{\mu \times f_i(\tau_i) + D_i}{\mu \times C_{17/20} + D_i} \quad (3.4)$$

Here, μ is the pulse shape determination factor, D_i is the dark hit rate for the i^{th} PMT and $C_{17/20}$ is the normalization constant for the 17 or 20 inch PMTs. The overall log-likelihood is given by the $\log(L) = \sum_i \log(\phi_i)$. The log-likelihood is maximized by the Newton-Raphson method, in which the x, y, z, T_0 are adjusted to the best-fit values, giving us the V2 reconstructed vertex.

3.2.5 Energy Reconstruction

Likelihood maximization is also used to reconstruct the energy of an event. A likelihood PDF is constructed using the number of hits, charge, and hit timing.

N_{hit} PDF

The expectation of the number of photons hitting PMT i, μ_i is a function of the visible energy and dark charge.

$$\mu_i = a_i(x, y, z) \times E_{vis} + d_i \quad (3.5)$$

Here, $a_i(x, y, z)$ is a coefficient that converts the event energy to the number of photons which is calibrated with the neutron events. It is determined by the PMT position x, y, z . d_i is the dark noise charge of PMT i, which is electronically measured. The probability that μ_i photons hit the i th PMT j times, k_{ij} , is ideally expressed by the poisson distribution:

$$k_{ij} = \frac{(\mu_i)^j}{j!} e^{-\mu_i} \quad (3.6)$$

However, in KamLAND waveform analysis, the 1 p.e. detection efficiency is reduced by the 0.3 p.e. software charge threshold. This threshold is set to reduce the acceptance of dark noise but also decreases hit detection efficiency. As a result, the PMT hit probability is reduced to:

$$P_{hit} = 1 - v_i e^{-\mu_i} \quad (3.7)$$

Hit Charge PDF

A Gaussian distribution is assumed for the hit charge PDF of each PMT:

$$f_{i,j(q_i)} = \frac{1}{\sqrt{2\pi j\sigma^2}} \exp\left(-\frac{(q_i - j)^2}{2j\sigma^2}\right) \quad (3.8)$$

q_i is the observed charge in p.e. units and σ is the charge resolution against 1 p.e. distribution.

Hit Time PDF

PMT hit timing factors into energy reconstruction by helping to discriminate hits unrelated to the physical event. The hit timing model is created using source calibration data.

$$P_{time,i} = \frac{\psi(t_i) a_i E_{vis} + d_i}{\mu_i} \quad (3.9)$$

The PDF is the sum of the signal hit distribution and the constant dark noise.

Energy Likelihood

The likelihood function to be maximized is constructed as

$$L = \prod_{Not\ hit\ PMTs} P_{no-hit,i} \prod_{Hit\ PMTs} \left[P_{hit,i} \left(\sum_{j=1}^{100} f_{i,j} \right) P_{time,i} \right] \quad (3.10)$$

The reconstructed energy is the one which maximizes this likelihood. The Newton-Raphson method is used to search for this energy. This process is implemented independently for the 17-inch PMTs and 20-inc PMTs, then the event energy is calculated with a weighting factor α :

$$E_{vis} = (1 - \alpha)E_{17inch} + \alpha E_{20inch} \quad (3.11)$$

The weighting factor $\alpha = 0.3$ was determined to maximizing energy resolution.

3.2.6 Bad Channels in Energy Reconstruction

The increase in the number of low gain PMTs has lead to worsening energy resolution over time, as these PMTs are excluded from the typical energy reconstruction described above. In particular, some of the low gain PMTs still detect photons, but proper gain calibration is not possible. A method for utilizing the information from operational low gain PMTs was developed, and the basic strategy is as follows:

1. The change in gain causes the effect of the 0.3 p.e. threshold on hit probability to change. The no-hit probability was expanded as follows:

$$P'_{no-hit,i} = \left(1 + \epsilon_1 \mu_i + \epsilon_2 \frac{\mu_i^2}{2!} + \epsilon_3 \frac{\mu_i^3}{3!} \right) e^{-\lambda \mu_i} \quad (3.12)$$

This model was originally a simple expansion of P_{no-hit} , but in the end was adjusted phenomenologically to better reproduce real data. This adjustment is why an additional $e^{-\lambda \mu}$ appears in the model.

2. The parameters $\epsilon_1, \epsilon_2, \epsilon_3$, and λ are estimated with actual data. The events satisfying the following selections are collected and the no-hit probability is calculated for each expected charge. The expected charge of the i-th PMT μ_i is estimated using the vertex and total charge of the events that meet the following conditions.

- $r < 6m$
- Not muons or events within 2 ms after muons
- Events with more than 120 17-inch PMT hits
- PMT waveforms that contain only 1 peak

Figure 3.6 shows the result of fitting this adjusted no-hit probability model. The fitting is performed run-by-run and for each PMT independently.

3. Use the updated no-hit probability pdf in the event energy reconstruction in Equation 3.10.

Making use of the low-gain PMTs can improve energy resolution by up to 3% [4]. Further analysis in this work uses energy reconstructed from the combination of normal and low-gain PMTs.

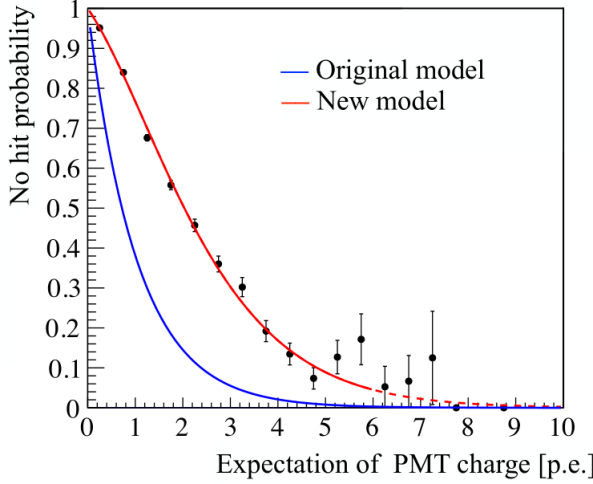


Figure 3.6: Fitting no hit probability to a low gain PMT against the expected charge μ . The original model is shown with the blue line while the red line is the new model which agrees better with low-gain PMT data.

3.2.7 Muon Reconstruction

The selection and understanding of muon and muon-correlated neutrons are essential to multiple background rejections. This section, describes the special selection criteria and reconstruction methods used for muons and neutrons.

Muon Selection Criteria

The muon event selection criteria are as follows:

- Total charge of 17inch PMTs, $Q_{17} \geq 10000$ p.e.
- $Q_{17geq} \geq 500$ p.e. and the number of hit OD PMTS ≥ 9 .

The former criteria selects muons which go through the scintillator volumes of the detector. A total charge of 10,000 p.e. roughly corresponds to an event energy of 30 MeV, which exceeds the energy range of most physical analyses in KamLAND-ZEN. The second selection is for muons that only deposit energy in the outer buffer oil (clipping muons). Muons passing through the buffer oil volumes do not scintillate, as

such the 500 p.e. threshold in Chrenkov radiation roughly corresponds to about 40 MeV of energy deposition.

3.2.8 Cosmic Ray Muon Reconstruction

Cosmic ray muon events form tracks as opposed to the point-like events caused by single decay events. The process is shown diagramattically in Figure ??

1. The ID PMT which detects the earliest light is identified. If the charge of this hit is low or isolated in time from the many other hits in the event, it is classed as a dark hit and ignored. A line is drawn from the earliest hit muon PMT and the center of the KamLAND detector. The intersection of this line and the outer balloon is marked as the temporary entrance point.
2. The PMT whose charge is the largest is identified. The brightest hit PMT should be hit later than the earliest PMT and the neighbors of the earliest PMTs. A line is drawn from the brightest hit PMT and the center of the KamLAND detector. The intersection of this line and the outer balloon is marked as the temporary exit.
3. The temporary track is defined as the line connecting the temporary entrance and exit. The temporary track is finally corrected by checking the correlation between the track length and the total charge.
4. The reconstruction quality is evaluated by checking the following:
 - Whether the earliest and the brightest PMTs can be identified
 - Whether the mean hit time of PMTs around the entrance is earlier than the around the exit.

A "badness" parameter value is assigned to the reconstruction according to this evaluation. With this evaluation, around 15% of muon candidates are

regarded as badly reconstructed though they can still be used in muon-neutron pairing. Bad muon reconstruction is caused by ringing in the PMT signals, muon bundles, and stopped muons.

The light yields in the muon events are estimated in [4]:

$$\langle dQ_C/dX \rangle = 28 \pm 5 \text{ p.e./cm (Cherenkov muons)} \quad (3.13)$$

$$\langle dQ_S/dX \rangle = 338 \pm 12 \text{ p.e./cm (Scintillation muons)} \quad (3.14)$$

3.2.9 MoGURA Neutron Reconstruction

Neutrons that are produced during cosmic ray spallation are best detected with the MoGURA DAQ due to the FBE's inability to handle the high after-pulse rate. After pulsing is also present in MoGURA and need to be rejected. An effective number of hits N_s was introduced. The neutron reconstruction procedures is as follows:

1. A 200ns wide time window is opened. The vertex is reconstructed using LT Vertex using the hit information contained in this window.
2. The times of flight to each PMT is calculated assuming the reconstructed vertex. Then the ToF subtracted hit timing distribution is obtained.
3. The obtained residual hit time distribution includes neutron capture 2.2 MeV gamma scintillation light and fake signals from after-pulses. To calculate the effective number of hits, N_{in} and N_{out} , the number of hits in a 30ns wide "ontime" window and a 170ns wide "offtime" window respectively are counted. N_s is then calculated as

$$N_s = N_{in} - N_{out} \times \frac{30\text{nsec}}{170\text{nsec}} \quad (3.15)$$

4. The ontine window is shifted by 20ns, the clock time of MoGDAQ, and step 3 is repeated.

5. The 200ns time window is shifted and steps 1-4 are repeated. the 200ns window and 30ns ontime window that maximizes N_s is found. The vertex given by the N_s maximizing time windows is taken as the reconstructed neutron capture event vertex.

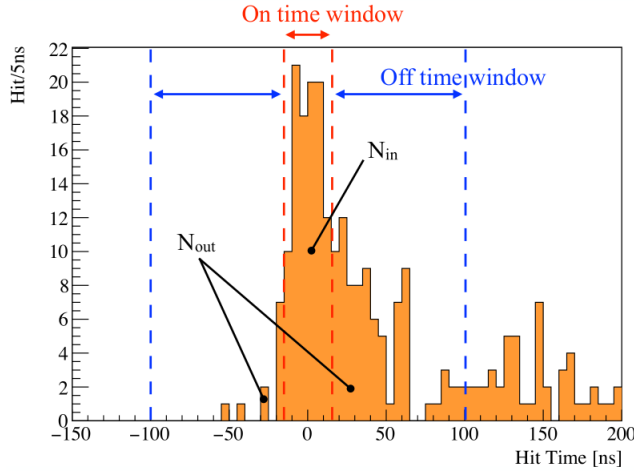


Figure 3.7: A neutron capture events hit times showing the contribution of fake after pulses and the time windows used to calculate N_s

3.2.10 Muon Neutron Correlation

The neutron selection process outlined above contains many noise events, thus the sample is only used in background discrimination when coincident with muons. In particular, MoGURA data neutrons are used to improve the rejection of xenon spallation products. The procedure for selecting muon-neutron pairs is:

1. Check the end unixtime of the previous KamDAQ run and the start unixtime of the current KamDAQ run.
2. Collect the MoGURA runs that collected data during this gap. Muon events collected by MoGURA are used in the gaps between KamDAQ runs, during KamDAQ runs muons collected with FBE data are used.

3. The delayed coincidence analysis is done to select neutron candidate events in a short time period after muons. The first cuts applied are on $dT > 2500\mu s$ and $N_s = N_{in} - N_{out} < 100$, these events are first removed. The subsequent MoGURA neutron selection criteria are outlined below.

The neutron selection in MoGURA is outlined in Figure 3.8. Two quantities are used, dT , the time delay between the neutron event and the previous muon, and N_s . From the 2D distribution, one sees that the event rate is higher in the short dT region due to noise and after-pulses. The N_s values also tend to be small due to signal loss caused by baseline overshoot in the PMTs. The following criteria were chosen to select MoGURA neutrons:

- $N_{total} = N_{in} + N_{out} > 150$ (Number of hit requirement)
- $N_s > 50 \wedge 10 < dT < 1200\mu s$ (reject after-pulses and accidental events)
- $!((N_s < dT(\mu s) + 70 \wedge 10 < dT < 20\mu s) || N_s < -0.8 \times dT(\mu s) + 106 \wedge 20 < dT < 70\mu s)$

Figure 3.9 shows the dT distribution of the MoGURA neutrons collected with the above criteria. The histogram is fitted to an exponential between 500 and 1000 μs , and the fitted function is extrapolated to the rest of the data range. The inefficiency of the neutron tag in the shorter dT period can be seen as the distribution turns off at low dT .

3.3 Event Selection

Candidate $0\nu\beta\beta$ events must pass several event selections. The selections are separated into non-physical events and background cuts. In this section, we first describe the event selections used in this analysis. Then, the impact of these selections on signal inefficiency are discussed.

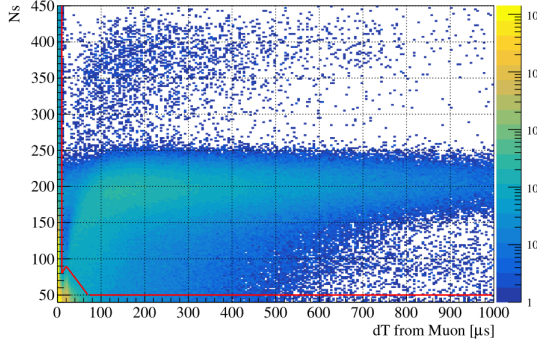


Figure 3.8: distribution showing the dT dependence of N_s . The events above the red line are selected as MoGURA neutrons and used for background rejection [9]

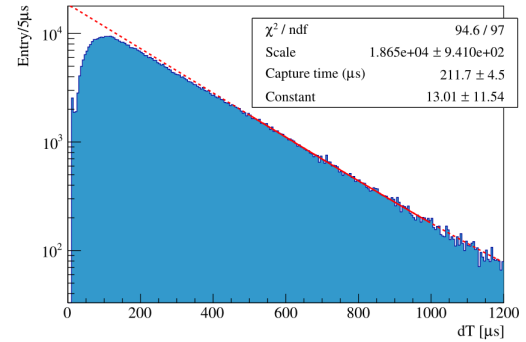


Figure 3.9: The dT distribution of selected MoGURA neutrons. The fit to an exponential is performed between 500 and 1000 μs . [9]

3.3.1 Unphysical and Bad Quality Event Rejection

Chapter 4

Conclusions

4.1 Summary of the thesis

Time to get philosophical and wordy.

Important: In the list of references at the end of thesis, abbreviated journal and conference titles aren't allowed. Either you must put the full title in each item, or create a List of Abbreviations at the beginning of the references, with the abbreviations in one column on the left (arranged in alphabetical order), and the corresponding full title in a second column on the right. Some abbreviations, such as IEEE, SIGMOD, ACM, have become standardized and accepted by librarians, so those should not be spelled out in full.

Appendix A

Proof of xyz

This is the appendix.

Bibliography

- [1] Nufit 5.0. available at <http://www.nu-fit.org>, 2020.
- [2] S. Abe, T. Araki, K. Chiba, T. Eda, M. Eizuka, Y. Funahashi, A. Furuto, A. Gando, Y. Gando, S. Goto, T. Hachiya, K. Hata, K. Ichimura, S. Ieki, H. Ikeda, K. Inoue, K. Ishidoshiro, Y. Kamei, N. Kawada, Y. Kishimoto, M. Koga, A. Marthe, Y. Matsumoto, T. Mitsui, H. Miyake, D. Morita, R. Nakajima, K. Nakamura, R. Nakamura, R. Nakamura, J. Nakane, T. Ono, H. Ozaki, K. Saito, T. Sakai, I. Shimizu, J. Shirai, K. Shiraishi, A. Suzuki, K. Tachibana, K. Tamae, H. Watanabe, K. Watanabe, S. Yoshida, S. Umebara, K. Fushimi, K. Kotera, Y. Urano, B. E. Berger, B. K. Fujikawa, J. G. Learned, J. Marićic, Z. Fu, S. Ghosh, J. Smolsky, L. A. Winslow, Y. Efremenko, H. J. Karwowski, D. M. Markoff, W. Tornow, S. Dell’Oro, T. O’Donnell, J. A. Detwiler, S. Enomoto, M. P. Decowski, K. M. Weerman, C. Grant, O. Penek, H. Song, A. Li, S. N. Axani, M. Garcia, and M. Sarfraz. Search for majorana neutrinos with the complete kamland-zen dataset, 2024.
- [3] Stefano Dell’Oro, Simone Marcocci, and Francesco Vissani. New expectations and uncertainties on neutrinoless double beta decay. *Phys. Rev. D*, 90:033005, Aug 2014.
- [4] Y. Karino. *Improvement of Background Rejection for Cosmic Muon Spallation in KamLAND-Zen*. PhD thesis, Tohoku University, 2017.
- [5] Leslie Lamport. *L^AT_EX—A Document Preparation System—User’s Guide and Reference Manual*. Addison-Wesley, 1985.
- [6] A. Li. *The Tao and Zen of neutrinos: neutrinoless double beta decay in KamLAND-ZEN 800*. PhD thesis, Boston University, 2020.
- [7] S. Matsuda. *Search for Neutrinoless Double-Beta Decay in ¹³⁶Xe after Intensive Background Reduction with KamLAND-Zen*. PhD thesis, Tohoku University, 2016.
- [8] H. Ozaki. *High Sensitivity Search for Neutrinoless Double-Beta Decay in KamLAND-Zen with Double Amount of ¹³⁶Xe*. PhD thesis, Tohoku University, 2019.
- [9] A. Takeuchi. *First Search for Majorana Neutrinos in the Inverted Mass Hierarchy Region with KamLAND-Zen*. PhD thesis, Tohoku University, 2023.

- [10] H. Yoshida. *Limit on Majorana Neutrino Mass with Neutrinoless Double Beta Decay from KamLAND-Zen*. PhD thesis, Tohoku University, 2014.

CURRICULUM VITAE

Joe Graduate

Basically, this needs to be worked out by each individual, however the same format, margins, typeface, and type size must be used as in the rest of the dissertation.